

How nucleation and luminosity shape faint dwarf galaxies

R. Sánchez-Janssen,¹★ T. H. Puzia,² L. Ferrarese,³ P. Côté,³ P. Eigenthaler,²
B. Miller,⁴ Y. Ordenes-Briceño,² E. W. Peng,⁵ K. X. Ribbeck,² J. Roediger,³
C. Spengler,^{2,5,6} M. A. Taylor.⁷

¹*UK Astronomy Technology Centre, Royal Observatory, Blackford Hill, Edinburgh, EH9 3HJ, UK*

²*Institute of Astrophysics, Pontificia Universidad Católica de Chile, Av. Vicuña Mackenna 4860, 7820436 Macul, Santiago, Chile*

³*NRC-Herzberg Astronomy and Astrophysics, 5071 West Saanich Road, Victoria, BC, V9E 2E7, Canada*

⁴*Gemini Observatory, Southern Operations Center, Casilla 603, La Serena, Chile*

⁵*Department of Astronomy and Kavli Institute for Astronomy and Astrophysics, Peking University, Beijing 100871, China*

⁶*Department of Physics and Astronomy, University of Victoria, Victoria, BC V8P 5C2, Canada*

⁷*Gemini Observatory, Northern Operations Center, 670 North A‘ohoku Place, Hilo, HI 96720, USA*

Accepted 2019 January 11. Received 2019 January 10; in original form 2018 November 1

ABSTRACT

We study the intrinsic shapes of a sample of over 400 quiescent galaxies in the cores of the Virgo and Fornax clusters with luminosities $10^6 \leq L_g/L_\odot \leq 10^8$. Similar to satellites of the Local Group and Centaurus A, these faint, low surface brightness cluster galaxies are best described as a family of thick ($\langle C/A \rangle > 0.5$), oblate-triaxial spheroids. However, the large sample size allows us to show that the flattening of their stellar distribution depends both on luminosity and on the presence of a nuclear star cluster. Nucleated satellites are thicker at all luminosities compared to their non-nucleated counterparts, and fainter galaxies are systematically thicker as well, regardless of nucleation. Once nucleation is accounted for, we find no evidence that the environment the satellites live in plays a relevant role in setting their three-dimensional structure. We interpret both the presence of stellar nuclei and the associated thicker shapes as the result of preferential early and rapid formation, effectively making these faint nucleated galaxies the first generation of cluster satellites.

Key words: galaxies: dwarf – galaxies: fundamental parameters – galaxies: structure – galaxies: clusters: individual (Virgo, Fornax, NGC 5128) – Local Group

1 INTRODUCTION

The three-dimensional (3D) shapes of galaxies provide constraints on the different physical mechanisms that play a role in the process of galaxy formation and assembly. Recent theoretical and numerical work indicates that the emergence of thin galactic discs is controlled by the gas fraction and the feedback from young stars, which in turn regulate star formation and chemical enrichment (Hayward & Hopkins 2017; Navarro et al. 2017; Ma et al. 2017). As a result of their burstier star formation histories, cold rotating discs assemble later in lower mass galaxies (Simons et al. 2017). At higher galaxy masses the contribution from dissipationless mergers grows significantly (Oser et al. 2010; Clauwens et al. 2017), and the resulting deposition of accreted stars leads to the emergence of spheroids, which notably exhibit a high degree of asphericity at the massive end (Holden et al. 2012; Foster et al. 2017; Krajnović et al. 2018; Li et al. 2018).

Major mergers are not relevant for the assembly of very low-mass galaxies (Fitts et al. 2018), but it is well established now that the stellar distributions of isolated $M_* \lesssim 10^9 M_\odot$ galaxies are significantly thicker than what is typical for rotating cold discs (Sánchez-Janssen et al. 2010; Roychowdhury et al. 2013). This suggests that in these systems dispersion support is dominant over rotation (Wheeler et al. 2017), and points towards feedback mechanisms setting the internal structure of low-mass centrals (Kaufmann et al. 2007). Explosive feedback episodes from supernovae and intense star formation act to dynamically heat preexisting stellar populations, thus driving stellar migration and thickening of the galactic bodies (Governato et al. 2010; Pontzen & Governato 2012; El-Badry et al. 2016). In the case of satellite dwarfs additional hydrodynamical and tidal interactions with their hosts can modify the structural and dynamical properties of low-mass systems, creating pressure-supported triaxial objects that in many aspects resemble the satellite populations of groups and clusters (Mastropietro et al. 2005; Smith et al.

★ E-mail: ruben.sanchez-janssen@stfc.ac.uk

2010; Kazantzidis et al. 2011, 2017; Lokas et al. 2012; but see Smith et al. 2015).

Until recently the 3D structure of faint satellites have been poorly studied. This is due primarily to their low luminosities and surface brightness levels, which limit the detail with which they can be studied. Because the orientation of individual galaxies in the sky is almost always unknown, the precise intrinsic shape of a given object can only be inferred by a combination of structural and kinematical data (Franx et al. 1991). The latter is extremely hard to obtain for faint systems, for which shapes are usually derived on statistical grounds via inversion or modelling of the apparent ellipticity distribution for an entire population (Sandage et al. 1970; Ryden & Terndrup 1994; Lisker et al. 2007, L07 hereafter). Naturally, the Local Group (LG) satellites are the best characterised population of low-mass galaxies. ‘Classical’ dwarf spheroidals ($M_V \lesssim -8.5$) are a class of relatively thick galaxies with intrinsic flattening ~ 0.5 and a certain degree of triaxiality (Salomon et al. 2015; Sánchez-Janssen et al. 2016; Sanders & Evans 2017). The advent of wide, deep imaging surveys has finally allowed mapping of larger volumes down to sufficiently low luminosities to enable comparable studies in populations of dwarf galaxies outside the LG (Ferrarese et al. 2012; Taylor et al. 2017; Danieli et al. 2017; Eigenthaler et al. 2018; Venhola et al. 2018). These datasets not only offer us the opportunity to study faint galaxies in other environments, but also with much larger number statistics than is possible locally—a critical aspect if one is to investigate how their properties depend on mass or galaxy type.

Beyond the simple distinction between star-forming and quiescent dwarfs, the latter class are known to be quite a diverse group of galaxies, with some subpopulations featuring the presence of nuclear star clusters (NSCs) or even disc-like features (L07). NSCs are compact stellar systems that in many aspects resemble typical globular clusters (GCs), but tend to be larger, more massive, and can host complex stellar populations, even in low-mass quiescent galaxies (Côté et al. 2006; Lisker et al. 2007; Turner et al. 2012; Paudel et al. 2011; Spengler et al. 2017). NSCs are found in galaxies of all morphological types, but tend to be particularly common in high-density environments. Indeed, in galaxy clusters like Virgo and Fornax, nucleation persists down to extremely low galaxy luminosities, $L_V \approx 10^6 L_\odot$ (Sánchez-Janssen et al. 2018; Ordenes-Briceño et al. 2018). Regardless of their exact formation mechanism, the presence of NSCs is indicative of past high-pressure star formation episodes, and thus provide clues on the formation of their host galaxy. Nucleated quiescent galaxies with stellar masses $\log(M_*/M_\odot) \approx 8-9$ have been shown to exhibit distinct clustering and phase-space properties (Ferguson & Sandage 1989) as well as to host the oldest stellar populations among all satellite subclasses (Schombert 2006; Lisker et al. 2008). Non-nucleated and nucleated intermediate-mass cluster satellites are best described as families of thick ($\langle C/A \rangle \approx 0.5$), nearly oblate spheroids, but the former subpopulation is known to be substantially flatter than the latter (Ryden & Terndrup 1994). L07 find that, at least for non-nucleated Virgo dEs, mass also seems to play a role, with fainter satellites being thicker than their more luminous counterparts.

In this contribution we take advantage of the present wealth of data on faint satellites outside the LG to show that these trends hold down to $L_V \approx 10^6 L_\odot$. The combined

sample size is large enough that it allows us, for the first time in this luminosity regime, to investigate shape differences as a function of brightness and nucleation.

2 SATELLITES IN THE LOCAL UNIVERSE

The galaxy samples used in this investigation come from the Next Generation Virgo Cluster Survey (Ferrarese et al. 2012, NGVS), the Next Generation Fornax Survey (Eigenthaler et al. 2018, NGFS), and the Survey of Centaurus A’s Baryonic Substructures (Taylor et al. 2017, SCABS). These studies have imaged these elliptical-dominated environments out to their respective virial radii, uncovering rich populations of mostly quiescent low-mass galaxies. Very detailed descriptions of the surveys are provided elsewhere, and here we only mention briefly the sample selection, the derivation of structural parameters, and the detection of nuclei.

The Virgo sample is identical to that presented in Sánchez-Janssen et al. (2016). Galaxies in the central $R \lesssim 0.2R_{\text{vir}}$ of the cluster are detected on *ugriz* images using a ring-median filter, and their two-dimensional light distributions are modelled as Sérsic (1968) functions with GALFIT (Peng et al. 2002). If the fit is not satisfactory due to the presence of an NSC, a second PSF-like component is included in the model. The identification of nucleated satellites is further complemented by a visual inspection of colour and unsharp-masked images of the galaxies (Sánchez-Janssen et al. 2018). We construct our sample of quiescent Virgo satellites from galaxies that have colours consistent with the cluster red sequence (Roediger et al. 2017).

Eigenthaler et al. (2018) present the properties of the dwarf galaxy population in the central $R \lesssim 0.25R_{\text{vir}}$ of Fornax. Galaxy detection is carried out by visual inspection of stacked *ugi* colour images, and candidates are selected according to their diffuse morphologies and for not showing evidence of ongoing star formation. Galaxies are also modelled with single-Sérsic components, and the fitting procedure is carried out iteratively using GALFIT. NSCs are identified visually as well, and in these cases a central mask is applied at each step of the fitting process to account for their presence.

The SCABS data cover an area $R \lesssim 0.5R_{\text{vir}}$ around NGC 5128/CenA (Taylor et al. 2017, 2018). The dwarfs were selected and their morphological parameters derived in an identical way to the NGFS (Ribbeck et al. 2019).

Finally, we use LG satellites as representatives of a lower-density environment. The parent sample comes from McConnachie (2012), but only systems within the zero-velocity surface of the LG are selected (see their Fig. 5). In addition, we only keep galaxies with low gas-mass fraction, $M_{\text{HI}}/L_V \leq 0.1 M_\odot/L_\odot$, which mimics our selection of quiescent cluster galaxies. The axis ratio measurements and their uncertainties are taken directly from McConnachie (2012).

We emphasise that the detection of NSCs in all samples is very robust. NSCs have much higher surface brightness than the underlying galaxy light, with a median $\Delta\mu = 2.4\text{mag}$ and $\sigma_{\Delta\mu} = 1.3\text{mag}$. The distribution of $\Delta\mu$ shows no dependence on q , and we detect NSCs across the entire range of observed axis ratios (see Fig. 1). Throughout this work we only use magnitudes and axis ratios measured in the *g*-band. Given that we use the same fitting function and code to model satellites in Virgo, Fornax and CenA, we

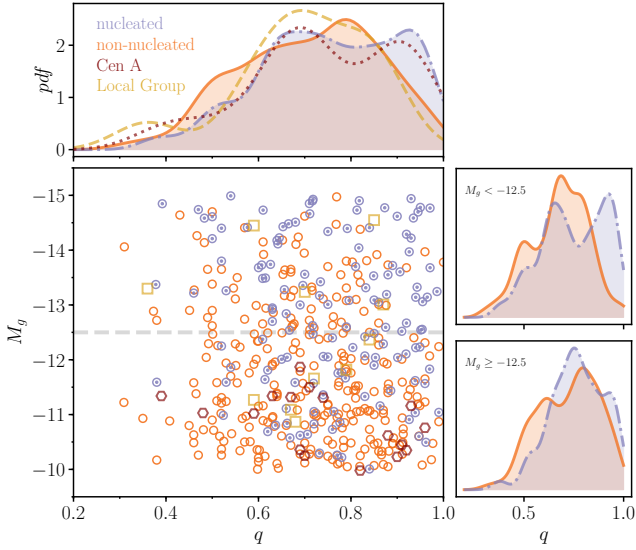


Figure 1. *Central panel:* Distribution of apparent axis ratios (q) and absolute magnitude (M_g) for dwarf galaxies in Virgo and Fornax (circles), CenA (hexagons) and the LG (squares). Open circles correspond to non-nucleated cluster dwarfs, whereas the galaxies hosting NSCs contain an inner dot symbol. The dashed horizontal line at $M_g = -12.5$ shows the division between the samples of bright and faint dwarfs. Notice the luminosity dependence of nucleation. *Top:* Probability distribution of apparent axis ratios for the four different populations of dwarfs. The paucity of apparently round non-nucleated dwarfs compared to nucleated ones is evident. *Right:* These two panels show, for dwarfs in Virgo and Fornax only, the axis ratio pdf for bright (top) and faint (bottom) non-nucleated (solid) and nucleated dwarfs (dot-dashed).

also apply the same $\langle\mu\rangle_e$ -dependent uncertainty for the axis ratio measurements of the two populations. The amplitude of these uncertainties is obtained from GALFIT modelling of simulated single-Sérsic galaxies, and it ranges from a minimum value of $\sigma_q = 0.02$ to 0.15 at $\langle\mu\rangle_e = 27.75$ mag arcsec $^{-2}$ (the NGVS 50% completeness limit). For all samples we impose the same criterion for low luminosity, $-15 \leq M_g \leq -10$, where we assume $(g - V) = 0.2$ for all LG satellites. The number of galaxies in each environment is shown in the second column of Table 1. We note that the Sagittarius dSph is the only LG satellite that satisfies all the above conditions and can be considered as nucleated. Only one of the CenA satellites hosts a nucleus, and in the following we treat all the group satellites essentially as a non-nucleated sample.

3 AXIS RATIO DISTRIBUTIONS

The central panel in Figure 1 shows the distribution of absolute magnitudes in the g -band and apparent axis ratios for dwarfs in Virgo and Fornax. We do not distinguish between the three populations, but focus on whether the dwarf exhibits an NSC (dot-circle symbols) or not (open circles). This is justified by our finding in Section 4 that the satellites in all environments have consistent intrinsic shapes. For reference, we also plot quiescent satellites in the LG (squares) and in CenA (hexagons). Two things are immediately obvious from this panel. First, and as already shown by Sánchez-Janssen

et al. (2018) for Virgo and Ordenes-Briceño et al. (2018) for Fornax, nucleation is a strong function of galaxy luminosity, with non-nucleated dwarfs being dominant towards fainter magnitudes. Second, the distributions of apparent axis ratios differ for nucleated and non-nucleated dwarfs. This is perhaps best appreciated in the top panel of Fig. 1, where we show the probability distribution function (pdf) for the nucleated (dot-dashed line) and the non-nucleated (solid) cluster satellites, and the non-nucleated group satellites (dashed and dotted lines for the LG and CenA, respectively). In all cases the pdf is a simple Gaussian kernel density estimation (kde) of the q distribution. The pdf for nucleated objects shows a peak for very round apparent axis ratios ($q \gtrsim 0.9$) that is absent from the corresponding distributions for non-nucleated cluster dwarfs and the LG objects. This is known to correspond to 3D shapes with low triaxiality.

The two panels at the right of Fig. 1 explore the luminosity dependence of the q distributions. The top panel corresponds to the bright subsample ($-15 \leq M_g < -12.5$), where the difference between nucleated and non-nucleated dwarfs is maximised. The pdf for the bright nucleated subsample is double-peaked, with maxima at $q \approx 0.65$ and $q \approx 0.95$. While the lower peak is also present in the pdf of non-nucleated dwarfs, their distribution falls rapidly towards high- q values. The behaviour of these two distributions is mimicked by their faint counterparts ($-12.5 \leq M_g < -10$; bottom panel), but the difference between the subsamples is less significant. Not only do the main peaks of the distributions shift towards higher q values, but the population of very round nucleated dwarfs is of relative lower importance.

4 INTRINSIC SHAPES INFERENCE

The analysis in the previous section provides a qualitative description of apparent shapes of nucleated and non-nucleated dwarfs at the very faint end of the galaxy luminosity function in nearby clusters and groups. We now attempt to model the observed axis ratio distributions in order to constrain their 3D shapes. We follow the methodology presented in Sánchez-Janssen et al. (2016), whereby galaxies are modelled as a family of optically thin triaxial ellipsoids. We assume that the 3D galaxy density is structured as a set of coaligned ellipsoids characterised by a common ellipticity $E = 1 - C/A$, and a triaxiality $T = (A^2 - B^2)/(A^2 - C^2)$, where $A \geq B \geq C$ are the intrinsic major, intermediate, and minor axes of the ellipsoid, respectively (Franx et al. 1991). The ellipticity and triaxiality parameters for the galaxy populations are assumed to be normally distributed, with means and standard deviations \bar{E} , σ_E , \bar{T} , and σ_T . We implement a Bayesian framework to explore the posterior distribution of the model parameters, which allows us to work directly on discrete data, and to account for individual, surface brightness-dependent axis ratio uncertainties. We use flat priors in the interval $[0, 1]$ for the location parameters of our model normal distributions (\bar{E} and \bar{T}). For the standard deviations σ_E and σ_T we adopt scale-invariant priors of the form $p(\sigma) \propto \sigma^{-1}$. We use the EMCEE code (Foreman-Mackey et al. 2013) to sample the posterior distribution of the parameters with 100 ‘walkers’ and 1000 steps—sufficient for the MCMC chains to reach equilibrium.

The results of this modelling are summarised in Ta-

Table 1. Intrinsic shapes of faint quiescent satellites. We show results for samples in Virgo, Fornax, CenA, and the LG. For the cluster populations we further differentiate between nucleated (N) and non-nucleated (nN) bright (b) and faint (f) satellites.

Sample	#	\bar{E}	σ_E	\bar{T}	σ_T
Virgo	228	$0.43^{+0.02}_{-0.02}$	$0.12^{+0.02}_{-0.01}$	$0.15^{+0.05}_{-0.05}$	$0.04^{+0.10}_{-0.02}$
Fornax	185	$0.46^{+0.02}_{-0.03}$	$0.13^{+0.03}_{-0.02}$	$0.24^{+0.46}_{-0.14}$	$0.13^{+0.19}_{-0.10}$
CenA	16	$0.43^{+0.08}_{-0.07}$	$0.15^{+0.08}_{-0.07}$	$0.26^{+0.46}_{-0.16}$	$0.07^{+0.19}_{-0.05}$
LG	11	$0.50^{+0.10}_{-0.08}$	$0.14^{+0.07}_{-0.06}$	$0.43^{+0.26}_{-0.24}$	$0.09^{+0.20}_{-0.07}$
bN	79	$0.42^{+0.03}_{-0.03}$	$0.14^{+0.04}_{-0.03}$	$0.11^{+0.10}_{-0.07}$	$0.05^{+0.11}_{-0.03}$
bnN	76	$0.50^{+0.03}_{-0.03}$	$0.12^{+0.03}_{-0.03}$	$0.57^{+0.18}_{-0.15}$	$0.09^{+0.22}_{-0.07}$
fN	58	$0.37^{+0.03}_{-0.03}$	$0.11^{+0.04}_{-0.03}$	$0.22^{+0.37}_{-0.12}$	$0.08^{+0.21}_{-0.06}$
fnN	200	$0.45^{+0.02}_{-0.02}$	$0.12^{+0.03}_{-0.02}$	$0.23^{+0.10}_{-0.11}$	$0.14^{+0.08}_{-0.11}$

ble 1, where we indicate the number of galaxies contributing to each subsample. The parameters for the preferred model correspond to the median and 68% confidence values of the marginalised posteriors. The first result is that satellites in Virgo and Fornax are very similar populations in terms of their 3D stellar distributions. The parameters in Table 1 correspond to intrinsic axis ratios of 1:0.95:0.57 and 1:0.91:0.54, respectively. It is well known that triaxiality distributions are not well constrained with photometric data alone (Binggeli 1980), and we will therefore focus the bulk of our analysis on the comparison of galaxy flattenings (\bar{E}). Nevertheless, it is worth mentioning that oblate-triaxial shapes are favoured in all cases over more prolate spheroids.

This structural similarity allows us to combine the Virgo and Fornax cluster samples to investigate the dependence of intrinsic shapes on galaxy luminosity and nucleation. As indicated in Fig. 1 and Table 1 we build four subsamples, with $M_g = -12.5$ serving as a dividing point between the bright (b) and faint (f) nucleated (N) and non-nucleated (nN) subpopulations. Despite the small subsample sizes the distributions of intrinsic ellipticity are remarkably well constrained in the range of $\bar{E} \approx 0.35$ –0.5. When analysing the nucleated and non-nucleated cluster populations separately there is a trend for the latter to have a higher degree of triaxiality than the former. This is consistent with the relative paucity of apparently round non-nucleated dwarfs (Fig. 1).

Fig. 2 summarises the main finding of this study, showing the intrinsic thickness C/A of all the subpopulations as a function of the median absolute magnitude of each subsample. X-axis error bars indicate the 16% and 84% percentiles of the magnitude distributions. Non-nucleated dwarfs, in spite of being a much thicker population than regular spiral discs, are more flattened (at $\gtrsim 2\sigma$) than nucleated systems at all luminosities. This is consistent with early findings for brighter non-nucleated and nucleated Virgo dEs (Ferguson & Sandage 1989; Ryden & Terndrup 1994; L07), but here we show that the structural differences hold down to the faintest luminosities where NSCs still occur. We also find that both nucleated and non-nucleated dwarfs are thicker as they become fainter. The trend with luminosity was already found in previous work on faint field and LG galaxies (Sánchez-Janssen et al. 2010), as illustrated in Fig. 2 with the inclusion of flattening measurements for faint dIrrs by Roychowdhury et al. (2013, triangles). It is remarkable

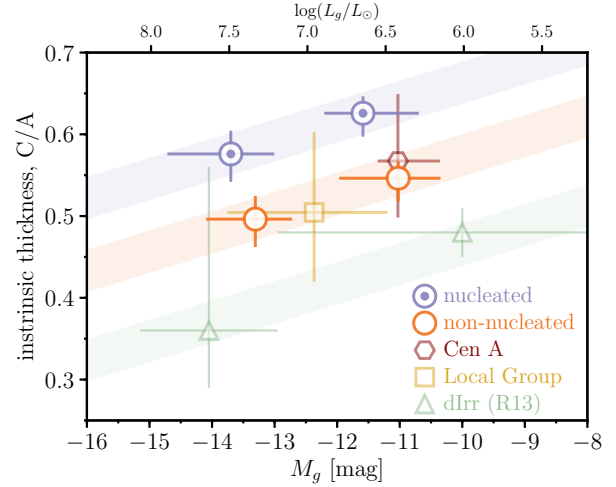


Figure 2. Intrinsic thickness as a function of absolute magnitude. Nucleated satellites are thicker at all luminosities compared to their non-nucleated counterparts, and fainter galaxies are systematically thicker as well, regardless of morphological type. Shaded regions show that different types of dwarfs exhibit similar trends with luminosity.

that the same behaviour holds in cluster environments, and separately for the nucleated and non-nucleated populations.

The dIrrs are the flattest subpopulation among the dwarfs, and this speaks to a structural difference between satellites and dwarfs that inhabit low environmental densities. However, the environmental dependence vanishes when we focus on satellites only and divide by morphological type (as traced by the presence of NSCs). This is demonstrated in Fig. 2 by the inclusion of the CenA (hexagon) and LG (square) satellites. Despite the small sample sizes, these (non-nucleated) group satellites have intrinsic flattenings fully consistent with the subsamples of non-nucleated cluster dwarfs at all luminosities. It seems that at these low masses nucleation has a larger impact on the intrinsic shapes of group and cluster satellites than the environment.

5 IMPLICATIONS AND CONCLUSIONS

The main finding in this study is that the intrinsic flattening of faint ($10^6 \lesssim L_g/L_\odot \lesssim 10^8$), quiescent satellites depends on galaxy luminosity and on nucleation, with the latter trend being slightly more significant than the former. Once these two parameters have been accounted for, we find no evidence that the environment the galaxies live in, be it Virgo, Fornax, CenA or the LG, plays a relevant role in setting their 3D structure. This suggests that either their stellar distributions are mainly shaped by internal mechanisms, or that becoming a satellite of a more massive halo is a sufficient requirement, with specific halo-dependent environmental effects having little influence on their shapes.

There is mounting evidence that faint galaxies form as thick, puffy systems (Wheeler et al. 2017). Star formation in low-mass haloes is expected to occur in episodic bursts at almost all redshifts (Muratov et al. 2015), and the associated

feedback-driven outflows pressurise gas and cause heating of the stellar orbits (Pontzen & Governato 2012; El-Badry et al. 2016). The progressively lower binding energies of fainter galaxies naturally allow for more impactful feedback effects and as a consequence the stellar distributions may become less flattened. The different intrinsic thickness of nucleated and non-nucleated cluster galaxies can also be explained by internal processes. The presence of compact stellar systems like NSCs and GCs is a clear indication that the host galaxies were actively forming stars at early cosmic times, when star formation rates (SFRs) and SFR surface densities were highest (Peng et al. 2008; Kruijssen 2015; Mistani et al. 2015). The notion that nucleated galaxies are a biased subpopulation is further supported by the observed strong clustering and old ages of the stellar populations of intermediate-mass nucleated dEs in Virgo (Ferguson & Sandage 1989; Lisker et al. 2008, 2009). As discussed above, this is accompanied by thicker intrinsic shapes compared to non-nucleated dEs, in the same way as found here for cluster satellites that are hundreds of times less luminous.

We therefore propose that the thicker shapes of nucleated faint galaxies in Virgo and Fornax are the result of preferential early and rapid formation. This is almost a necessity for objects that inhabit the inner cluster regions, for which typical infall times are of the order of several billion years. But in this scenario the nucleated objects would be the most biased subpopulation, truly representing the first generation of cluster satellites. A clear prediction from this hypothesis is that nucleated faint satellites should show evidence for enhanced abundance ratios compared to non-nucleated objects, which would be indicative of a formation history dominated by early intense starbursts (Liu et al. 2016). Early formation not only is characterised by explosive feedback events that result in a higher degree of dispersion support and thicker stellar distributions, but these early infallers have also spent a substantial amount of time in the central cluster environment, where more frequent and intense tidal interactions can further heat the stellar orbits (Kazantzidis et al. 2011; Smith et al. 2015). While these mechanisms are arguably at place, it is important to note that some of the difference in flattening between satellites and dIrrs is almost certainly caused by the sustained stellar mass growth of the field dwarfs. The deepening of the potential together with the reduced gas accretion rates at more recent epochs result in weaker stellar feedback effects (Muratov et al. 2015), and this favours the development of stable and calm gas discs that are self-regulated by continuous star formation.

REFERENCES

- Binggeli B., 1980, *A&A*, 82, 289
- Clauwens B., Schaye J., Franx M., Bower R. G., 2017, *MNRAS*, 000, 1
- Côté P., et al., 2006, *ApJS*, 165, 57
- Danieli S., van Dokkum P., Merritt A., Abraham R., Zhang J., Karachentsev I. D., Makarova L. N., 2017, *ApJ*, 837, 136
- Eigenthaler P., et al., 2018, *ApJ*, 855, 142
- El-Badry K., Wetzel A., Geha M., Hopkins P. F., Kereš D., Chan T. K., Faucher-Giguère C.-A., 2016, *ApJ*, 820, 131
- Ferguson H., Sandage A., 1989, *ApJ*, 346, L53
- Ferrarese L., et al., 2012, *ApJS*, 200, 4
- Fitts A., et al., 2018, *MNRAS*, 479, 319
- Foreman-Mackey D., Hogg D., Lang D., Goodman J., 2013, *PASP*, 125, 306
- Foster C., et al., 2017, *MNRAS*, 472, 966
- Franx M., Illingworth G., de Zeeuw T., 1991, *ApJ*, 383, 112
- Governato F., Brook C., Mayer L., al. E., 2010, *Nature*, 463, 203
- Hayward C. C., Hopkins P. F., 2017, *MNRAS*, 465, 1682
- Holden B., van der Wel A., Rix H.-W., Franx M., 2012, *ApJ*, 749, 96
- Kaufmann T., Wheeler C., Bullock J. S., 2007, *MNRAS*, 382, 1187
- Kazantzidis S., Lokas E., Callegari S., Mayer L., Moustakas L., 2011, *ApJ*, 726, 98
- Kazantzidis S., Mayer L., Callegari S., Dotti M., Moustakas L. A., 2017, *ApJ*, 836, L13
- Krajinović D., Emsellem E., den Brok M., Marino R. A., Schmidt K. B., Steinmetz M., Weilbacher P. M., 2018, *MNRAS*, 477, 5327
- Kruijssen J. M. D., 2015, *MNRAS*, 454, 1658
- Li H., Mao S., Cappellari M., Graham M. T., Emsellem E., Long R. J., 2018, *ApJ*, 863, L19
- Lisker T., Grebel E. K., Binggeli B., Glatt K., 2007, *ApJ*, 660, 1186
- Lisker T., Grebel E., Binggeli B., 2008, *AJ*, 135, 380
- Lisker T., et al., 2009, *ApJ*, 706, L124
- Liu Y., et al., 2016, *ApJ*, 818, 179
- Lokas E., Majewski S., Kazantzidis S., Mayer L., Carlin J., Nidever D., Moustakas L., 2012, *ApJ*, 751, 61
- Ma X., et al., 2017, *MNRAS*, 467, 2490
- Mastropietro C., Moore B., Mayer L., Debattista V., Piffaretti R., Stadel J., 2005, *MNRAS*, 364, 607
- McConnachie A. W., 2012, *AJ*, 144, 4
- Mistani P. A., et al., 2015, *MNRAS*, 455, 2323
- Muratov A. L., Kereš D., Faucher-Giguère C.-A., Hopkins P. F., Quataert E., Murray N., 2015, *MNRAS*, 454, 2691
- Navarro J. F., et al., 2017, *MNRAS*, 000, 1
- Ordenes-Briceño Y., et al., 2018, *ApJ*, 860, 4
- Oser L., Ostriker J. P., Naab T., Johansson P. H., Burkert A., 2010, *ApJ*, 725, 2312
- Paudel S., Lisker T., Kuntschner H., 2011, *MNRAS*, 413, 1764
- Peng C., Ho L., Impey C., Rix H.-W., 2002, *AJ*, 124, 266
- Peng E. W., et al., 2008, *ApJ*, 681, 197
- Pontzen A., Governato F., 2012, *MNRAS*, 421, 3464
- Roediger J. C., et al., 2017, *ApJ*, 836, 120
- Roychowdhury S., Chengalur J., Karachentsev I., Kaisina E., 2013, *MNRAS*, 436, L104
- Ryden B., Terndrup D., 1994, *ApJ*, 425, 43
- Salomon J.-B., Ibata R., Martin N., Famaey B., 2015, *MNRAS*, 450, 1409
- Sánchez-Janssen R., Méndez-Abreu J., Aguerri J. A. L., 2010, *MNRAS*, 406, no
- Sánchez-Janssen R., et al., 2016, *ApJ*, 820, 69
- Sánchez-Janssen R., et al., 2018, arxiv:1812.01019
- Sandage A., Freeman K., Stokes N., 1970, *ApJ*, 160, 831
- Sanders J. L., Evans N. W., 2017, *MNRAS*, 472, 2670
- Schombert J., 2006, *AJ*, 131, 296
- Sérsic J., 1968, Atlas de galaxies australes. Cordoba, Argentina: Observatorio Astronomico, 1968
- Simons R. C., et al., 2017, *ApJ*, 843, 46
- Smith R., Davies J., Nelson A., 2010, *MNRAS*, 405, 1723
- Smith R., et al., 2015, *MNRAS*, 454, 2502
- Spengler C., et al., 2017, *ApJ*, 849, 55
- Taylor M. A., et al., 2017, *MNRAS*, 469, 3444
- Taylor M. A., et al., 2018, *ApJ*, 867, L15
- Turner M. L., Côté P., Ferrarese L., Jordán A., Blakeslee J. P., Mei S., Peng E. W., West M. J., 2012, *ApJS*, 203, 5
- Venhola A., et al., 2018, pp 1–31
- Wheeler C., et al., 2017, *MNRAS*, 465, 2420

This paper has been typeset from a \TeX/L\AA\TeX file prepared by the author.